WAVELET APPLICATIONS FOR FLIGHT FLUTTER TESTING

Rick Lind[1], Marty Brenner[2], and Lawrence C. Freudinger[3]
NASA Dryden Flight Research Center

Abstract

Wavelets present a method for signal processing that may be useful for analyzing responses of dynamical systems. This paper describes several wavelet-based tools that have been developed to improve the efficiency of flight flutter testing. One of the tools uses correlation filtering to identify properties of several modes throughout a flight test for envelope expansion. Another tool uses features in time-frequency representations of responses to characterize nonlinearities in the system dynamics. A third tool uses modulus and phase information from a wavelet transform to estimate modal parameters that can be used to update a linear model and reduce conservatism in robust stability margins.

1. Introduction

Flight flutter testing for envelope expansion is a time-consuming and dangerous procedure because of the relative inefficiency of traditional methods. The most common of these methods is to track damping of structural modes throughout the envelope and predict the onset of flutter through decreases noted in the corresponding trends [11]. The danger with this method, and therein the main cause of inefficiency, is the possibility of unexpectedly encountering a flutter instability as a result of sudden changes in damping that are not indicated by trends. Thus, the envelope is expanded using small increments in flight condition that reduce the possibility of such an occurrence.

NASA Dryden Flight Research Center has been developing tools to increase the efficiency of flight flutter testing by reducing the required amount of flight time while simultaneously increasing safety to aircraft and crew [15]. These tools encompass several areas of flight flutter testing ranging from excitation to data transfer to stability prediction. In particular, tools have been formulated that use wavelets to accurately analyze the types of data that are typically measured during flight flutter testing.

[1] Aerospace Engineer, Structural Dynamics, Edwards CA 93523, *rick.lind@dfrc.nasa.gov*, 661.258.3075
[2] Aerospace Engineer, Structural Dynamics, Edwards CA 93523, *martin.brenner@dfrc.nasa.gov*
[3] Aerospace Engineer, Structural Dynamics, Edwards CA 93523, *lawrence.freudinger@dfrc.nasa.gov*

Wavelets represent a type of processing that relaxes several constraints on the signal that are assumed to be satisfied when using traditional Fourier processing [24]. The wavelet transform has been used for a wide variety of signal and image processing applications; however, its use for dynamical systems, and particularly flight flutter testing, has been somewhat more limited to applications such as denoising in the time-frequency domain [3, 7].

A tool has been developed recently to use wavelets as basis functions for a correlation filter that identifies modal properties [8]. This tool uses inner products between data and a set of wavelets as a measure of correlation. The modal properties of the system are then identified by noting the associated properties of the wavelets that are highly correlated with the data.

Another wavelet-based tool that has been recently developed uses wavelet maps to extract information about nonlinearities in system dynamics [16, 17]. This tool considers features and trends in the time-domain representations of transient responses to indicate the presence of nonlinearities. Furthermore, these features and trends can be exploited to characterize the nature of the nonlinearities.

A third tool uses wavelets for parametric estimation of modal dynamics and state-matrix elements [4]. This tool is developed in conjunction with a flutter analysis tool such that the parameter estimates are incorporated into the analysis to reduce the amount of modeling error considered by robust stability metrics [12]. This tool is especially appropriate for flight flutter testing by considering an on-line formulation of the tool that estimates modal parameters during flight [5].

This paper presents these wavelet-based tools that have recently been developed for use during flight flutter testing. These tools have been previously documented; therefore, the purpose here is to present a summary and compendium of the recent advances.

This paper is divided into 3 main sections such that each section is devoted to a particular tool. The discussion is limited for brevity to the basic theoretical foundation and an example to demonstrate each tool in a flight test context. References are listed that can be consulted to obtain more extensive information.

2. Correlation Filtering

This section presents the wavelet-based tool for correlation filtering. Laplace wavelets are introduced in terms of damping and natural frequency to represent basis functions for the tool. The filtering uses these functions to generate a correlation coefficient and indicate modal parameters of the system. The tool is demonstrated by filtering data from an envelope expansion flight test.

2.1. Laplace Wavelet

The Laplace wavelet, ψ, is a complex, analytic, single-sided damped exponential.

$$\psi_\gamma(t) = \begin{cases} Ae^{-\frac{\zeta}{\sqrt{1-\zeta^2}}\omega(t-\tau)}e^{-j\omega(t-\tau)} & : t \in [\tau, \tau+T] \\ 0 & : \text{else} \end{cases}$$

The parameter vector, $\gamma = \{\omega, \zeta, \tau\}$, determines the wavelet properties. These parameters are related to modal dynamic properties by associating ω with frequency, ζ with viscous damping ratio, and τ as a time index. The coefficient A is an arbitrary factor used to scale each wavelet to unity norm. The range, T, ensures the wavelet is compactly supported.

This function is called a Laplace wavelet to emphasize that its derivation is related to the Laplace transform. In particular, the Laplace wavelet has a strong similarity to the inverse Laplace transform of the transfer function for an underdamped, second-order system. Thus, the Laplace wavelet is generated by considering features anticipated in mechanical system responses.

2.2. Laplace Wavelet Dictionary

The analysis of response data from dynamical systems often uses assumptions of linearity such that the system response should be a linear combination of subsystem responses [10]. These subsystems are second-order single degree of freedom systems in the case of modal analysis. Signal decomposition of the response into the subsystem responses for steady-state data can be accomplished via Fourier transforms which use a basis of infinite length sinusoids of varying frequencies.

Transient response data are difficult to effectively decompose even for linear systems since the system response is composed of subsystem responses with time-varying magnitudes. The basis of infinitely long sinusoids used by the Fourier transform is not ideal for this nonstationary data. Wavelets may be used for signal decomposition of transient response data since they inherently allow time-varying magnitudes of the subsystem responses.

The concept of a dictionary is introduced to describe a set of wavelets used for signal decomposition [24]. This dictionary is distinguished from a basis since the response of any dynamical system may not necessarily be expressed as a linear combination of the finite number of entries in the dictionary. The dictionary approximates a basis assuming the responses to be analyzed are similar in nature to the Laplace wavelets. The dictionary is basically a database of waveforms.

A finite set of wavelet parameters is used to generate the dictionary. A discrete gridding of the parameter space results in sets $\Omega, \mathcal{Z}$ and $\mathcal{T}$.

$$\begin{aligned} \Omega &= \{\omega_1, \omega_2, \ldots, \omega_p\} \subset \mathcal{R}_+ \\ \mathcal{Z} &= \{\zeta_1, \zeta_2, \ldots, \zeta_q\} \subset \mathcal{R}_+ \cap [0, 1) \\ \mathcal{T} &= \{\tau_1, \tau_2, \ldots, \tau_r\} \subset \mathcal{R} \end{aligned}$$

The dictionary is defined for the set of Laplace wavelets whose parameters are contained in these sets as denoted by $\gamma \in \Omega \times \mathcal{Z} \times \mathcal{T}$.

2.3. Filtering Approach

An inner product operation measures the correlation between signals. Correlating a signal, $f(t)$, with a Laplace wavelet, $\psi_\gamma(t)$, measures similarity between frequency and damping properties of the wavelet and the system that generated the signal.

A correlation coefficient, $\kappa_\gamma \in \mathcal{R}$, is defined to quantify the degree of correlation between the wavelet and a time signal. This correlation coefficient considers the angle between the vectors such that the maximum coefficient results from correlating parallel vectors.

$$\kappa_\gamma = \sqrt{2}\frac{|< \psi_\gamma, f(t) >|}{\|\psi_\gamma\|_2 \|f\|_2}$$

κ_γ is a matrix whose dimensions are determined by the parameter vectors of $\{\omega, \zeta, \tau\}$. A useful correlation coefficient $\kappa(\tau)$ is defined for on-line modal analysis to correlate frequency and damping at each time value. Peaks of the surface plot of κ_γ for a given τ relate the wavelets with the strongest correlation to the data. Define $\kappa(\tau)$ as the peak values of κ_γ at each τ and define $\bar{\omega}$ and $\bar{\zeta}$ as the parameters of the Laplace wavelet associated with the peak correlation.

$$\kappa(\tau) = \max_{\substack{\omega \in \Omega \\ \zeta \in \mathcal{Z}}} \kappa_\gamma = \kappa_{\{\bar{\omega}, \bar{\zeta}, \tau\}}$$

A normalizing factor of $\sqrt{2}$ allows $\kappa(\tau) = 1$ when the signal in some time interval T is a linear combination of the real and imaginary components of a particular wavelet. The formulation of $\kappa(\tau)$ searches for a maximum value across values of ω and ζ. This search can use subsets of Ω and $\mathcal{Z}$ to find local maxima and compute a κ vector at each time index. The subset searching is analogous to finding multiple peaks of interest on a frequency spectrum plot, with the added variables of damping and time.

The support range T is not explicitly used to define κ but it can greatly affect the computed value. Small T

may increase κ for signals not strongly correlated while large T may decrease κ to the noise floor even for signals which are strongly correlated. Thus, T can not be chosen arbitrarily. Knowledge of crest factors, signal-to-noise ratios, and effective decay rates observed in the data can all be used in guiding the choice of T.

A correlation filter approach computes the κ vector for a response signal. The dampings $\bar{\zeta}$ and frequencies $\bar{\omega}$ associated with peak κ values indicate the modal properties of the system which generated the data. This filter acts as a transform from the time domain to a modal parameter, or stability, domain. This stability estimate should be representative of the modal properties of the system if the data represent a linear, time-invariant system in free decay.

2.4. Flight Data Analysis

Application to actual aircraft data is required to evaluate Laplace wavelet correlation filtering for use in a flight test environment. Consider the DAST aircraft (Drones for Aerodynamic and Structural Testing), a remotely piloted research drone which encountered explosive flutter in June 1980 [9].

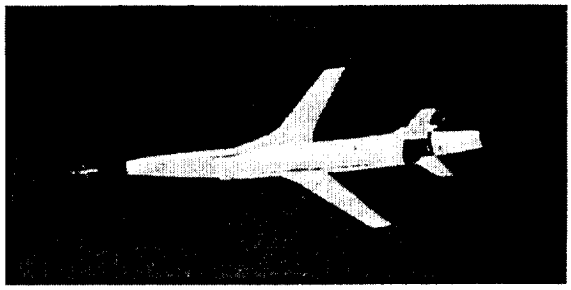

Figure 1: NASA DAST vehicle in flight

The last 40 s of flight data demonstrate the transition from stable flight to the onset of flutter and thus are of interest for evaluating correlation filtering. This data corresponds to flight at 15,000 ft over which the Mach number varies between approximately 0.80 and 0.825. Wingtip accelerations are measured at 500 Hz in response to symmetric aileron pulses and are used to analyze modal properties of the vehicle. A flutter suppression controller was engaged during this flight; however, the vehicle encountered a flutter instability due to an implementation error.

The response data was correlated with a Laplace dictionary based on support $T = 2$ s. The starting time indices for filtering, τ, are data dependent and correspond to local maxima with an emphasis on transient excursions. The remaining elements of the dictionary are members of the sets Ω and Z.

$$\begin{aligned} \Omega &= \{10 : 0.25 : 30\} \\ \mathcal{Z} &= \{0 : 0.003 : 0.063\} \end{aligned}$$

The results of correlation filtering are presented in Figure 2. Figure 2a presents the acceleration response of the left wingtip while Figures 2b, 2c, and 2d present the peak correlation, frequency, and damping values as a function of time. A threshold $\kappa(\tau) > 0.8$ is applied to avoid clutter on the plot without discarding interesting information.

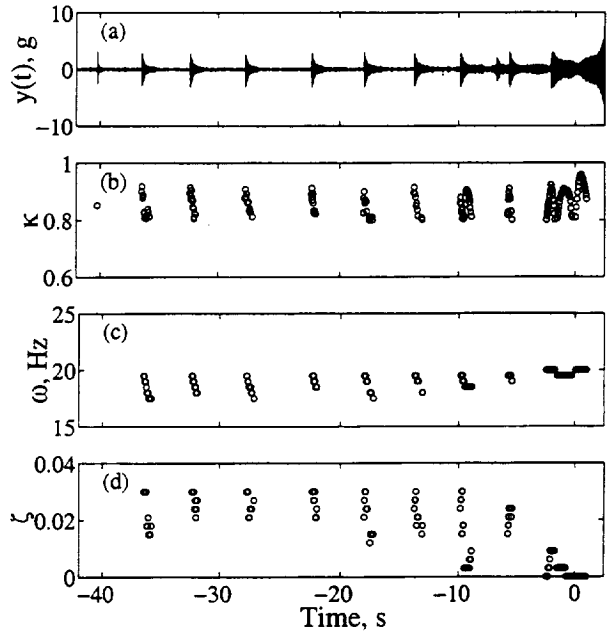

Figure 2: Correlation Filtering of the DAST Data with the Laplace Wavelet Dictionary: Left Wingtip Acceleration (a), Peak Correlation Values $\kappa(\tau) > 0.8$ (b), Wavelet Frequencies Associated with Peak Correlations (c), Corresponding Wavelet Damping Values (d)

Classical flutter testing uses trend analysis based on grouping correlations for a given pulse into an average value. The results from performing this operation on the data in Figure 2 are presented in Table 1.

t, s	$\bar{\zeta}$	$\bar{\omega}$, Hz
−36	0.035	18.25
−32	0.030	18.75
−27	0.027	19.0
−22	0.026	19.0
−17	0.025	19.2
−13	0.022	19.0
−9	0.025/0.009	19.5/18.5
−5	0.018/0.0	19.5/18.5
−2	0.005	19.7
−1	0.000	19.7

Table 1: Frequency and Damping Values Estimated by Correlation Filtering

As can be seen in both Figure 2 and Table 1, the average frequency and damping values show a roughly steady trend until the impulse at $t = -13s$ at which time the dominant frequency edges up slightly by 0.5 Hz and the damping tends toward zero. From $t = -9s$ and later, a progressive increase in residual dynamics observed in Figure 2a indicates the arrival of the stability boundary. As the frequency spread converges to a single frequency, the damping values converge to zero. These estimates agree with previous parameter estimation results [1].

This analysis demonstrates that frequency and damping estimates provided by Laplace wavelet analysis are a diagnostic tool useful for free decay analysis because it provides time-varying estimates at arbitrary resolutions, which are not available from Fourier or traditional linear estimation techniques. This information is particularly useful in cases such as the DAST where pulse responses of closed-loop systems are observed specifically with the intent of tracking modal dynamics in the time domain.

3. Analyzing Nonlinearities

This section discusses the tool that uses wavelets to analyze nonlinearities. This tool generates a time-frequency representation of a signal and then uses associated dominant features to indicate information about nonlinearities in the dominant dynamics. Responses from linear and nonlinear pitch-plunge systems are analyzed to demonstrate how nonlinearities are detected and characterized with this tool.

3.1. Extracting Dominant Scales

Wavelet maps can sometimes be difficult to interpret because of the large amount of information contained in this two-dimensional representation. Many applications are only interested in the dominant components of a signal and consequently are only interested in the dominant information from these maps. One method of extracting dominant information is to identify the scales associated with peaks in the wavelet maps, $F(\tau, a)$, that are associated with the Morlet wavelet [24].

Consider a vertical strip $F(t_i, a)$ that represents the magnitude of the correlations between the signal $f(t)$ and wavelets at position $\tau = t_i$ for the vector of scales $a \in A$. Define $\overline{F_i}$ as the maximum peak magnitude correlation for this strip which corresponds to a wavelet with scale defined as $\overline{a_i} \in A$.

$$\overline{F_i} = F(t_i, \overline{a_i}) = \max_{a \in A} F(t_i, a) = \max_{a \in A} F(\tau, a)\Big|_{\tau = t_i}$$

The parameter $\overline{a_i}$ can be utilized to determine sample length period of the dominant wavelet pattern in the data. This periodicity can be interpreted as a measure of the dominant sinusoidal frequency component in the response data under the approximations that the Morlet wavelet is essentially sinusoidal in nature. Thus, the dominant scale is loosely related to the well-known concepts of ridges and instantaneous frequency [23].

Values of $\overline{a_i}$ are computed at each instant of time to produce a time-varying measure of dominant scale and frequency; however, there are instances when no value can be computed. For example, the real Morlet wavelet will be alternating from in-phase to out-of-phase with a sinusoidal signal and so there will be instances when the wavelet does not correlate well with the signal. The possible misinformation that could result from this is eliminated by applying a threshold factor that ignores portions of the wavelet map with no noticeable energy or low correlation factor.

3.2. Nonlinear Testbed

An aeroelastic testbed is used at Texas A&M University for flutter research using a prototypical aeroelastic wing section. This system allows pitch-plunge motion to represents the bending-torsion motion that is often association with a classical flutter mechanism.

Nonlinearities are introduced to the system dynamics through the stiffness associated with pitch movement. This stiffness is described by a nonlinear polynomial function of the pitch angle. Such structural nonlinearities occur in physical aeroelastic systems and have been investigated to determine their effect on inducing limit cycle oscillations [6].

Models of the Texas A&M aeroelastic system are formulated using three types of stiffness functions to investigate a variety of behaviors related to different nonlinearities. These functions associated with the pitch stiffness are chosen to represent a linear spring, a nonlinear hardening spring, and a nonlinear softening spring.

The linear spring constant is denoted k_{lin}.

$$k_{lin} = 2.82$$

The softening spring function is denoted k_{soft}.

$$k_{soft} = 2.82 - 200\alpha^2 + 10000\alpha^4$$

The hardening spring function is denoted k_{hard}.

$$k_{hard} = 2.82 - 62.3\alpha + 3709.7\alpha^2 - 24196.0\alpha^3 + 48757\alpha^4$$

The models with each of these springs can be linearized around the equilibrium condition at the phase-plane origin by eliminating higher-order terms in α. Each linearized model is identical and has a pitch-mode natural

frequency at 1.29 *Hz*. Thus, the the linear and nonlinear systems at stable flight conditions should behave similarly for responses with small α values.

3.3. Pitch Responses

Simulated free-decay responses are computed for each nonlinear model using a 4^{th} order Runge-Kutta algorithm to integrate the equations of motion with a time step of .001 *s*. The pitch responses are shown in Figure 3.

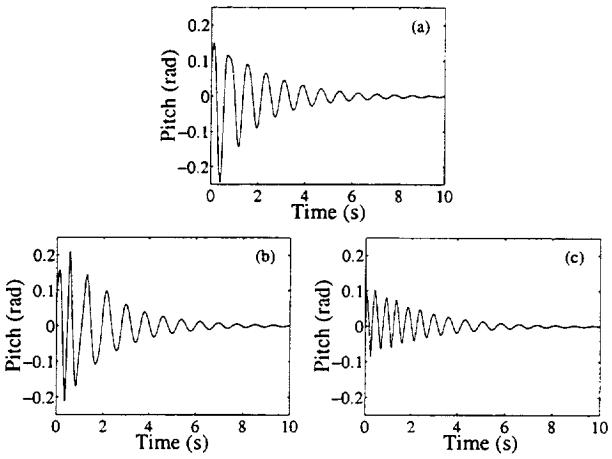

Figure 3: Simulated Time Responses of the Pitch Angle of Each Model at Airspeed U=8 m/s : Linear k_{lin} (a), Nonlinear Softening k_{soft} (b), Nonlinear Hardening k_{hard} (c)

The plunge responses are not presented here because they are not used for the current analysis. The plunge mode has a higher damping than the pitch mode and consequently the plunge response decays quickly to zero. Conversely, the pitch motion continues with a magnitude that is sufficient to demonstrate properties of the dynamics and so the analysis will focus only on the pitch response.

Time-scale information is obtained by computing the continuous wavelet transform of these time responses. Figure 4 presents the maps $F(\tau, a)$ generated by a wavelet analysis on the pitch data using real Morlet wavelet basis functions.

Figure 4 shows 2-dimensional plots of the 3-dimensional wavelet maps. The correlation magnitude between the wavelet and signal at each position and scale value is represented by a shade of gray with white implying low correlation and black implying high correlation. Such a shading approach is not optimal for representing these wavelet maps since several closely spaced scales will often appear to have a similar correlation magnitude and the resulting signal decomposition appears to be spread over these scales; however the 3-dimensional images are often more difficult to display.

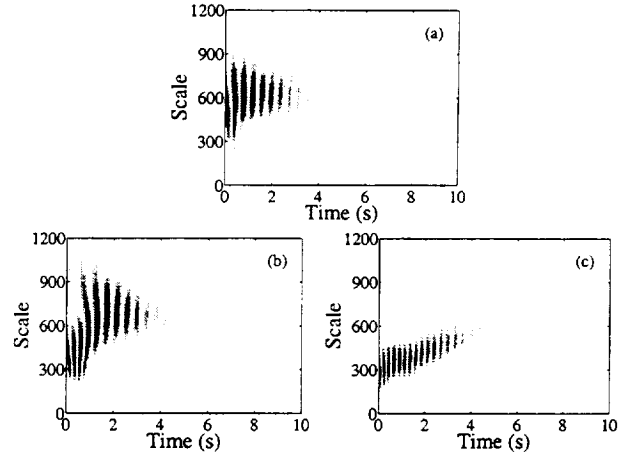

Figure 4: Wavelet Transform Maps of the Pitch Data Obtained from the Models Simulated at Airspeed U=8 m/s : Linear k_{lin} (a), Nonlinear Softening k_{soft} (b), Nonlinear Hardening k_{hard} (c)

3.4. Detecting Nonlinearities

The detection and characterization of nonlinearities affecting the system dynamics is difficult based on the general time responses of Figure 3 and corresponding time-frequency maps of Figure 4. The concept of dominant scales is therefore introduced as a means to extract the most important information and simplify the analysis of nonlinearities.

Figure 5 presents the plots of $\overline{a_i}$ corresponding to the peak magnitude wavelets from the maps of Figure 4.

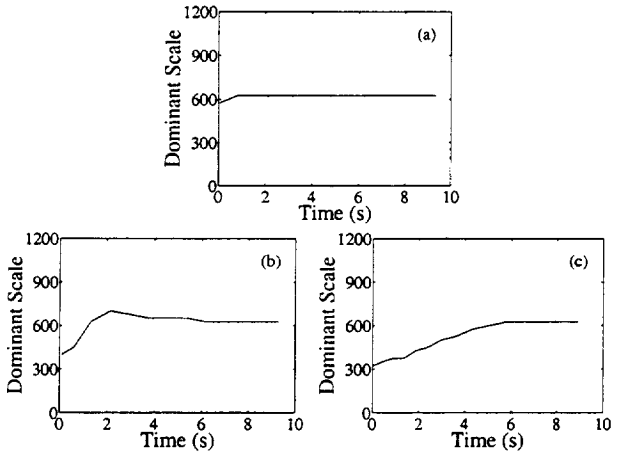

Figure 5: Scale $\overline{a_i}$ Corresponding to Peaks of the Wavelet Transform Maps of the Pitch Data Obtained from the Models Simulated at Airspeed U=8 m/s : Linear k_{lin} (a), Nonlinear Softening k_{soft} (b), Nonlinear Hardening k_{hard} (c)

The wavelet maps in Figure 4 and the scales $\overline{a_i}$ corresponding to the peaks of those maps in Figure 5 show clear differences in the responses from each spring. These plots may not be immediately obvious to interpret; how-

ever, a careful examination reveals the wavelet analysis presents information which can be directly compared to properties of the dynamical systems. Interpretation is aided by referring to convenient regions of the time response.

Region I	$0 < t < 2\ s$
Region II	$2 < t < 7\ s$
Region III	$7 < t < 10\ s$

Consider the wavelet information from Region I corresponding to the responses for $t < 2\ s$. This portion of the responses from each system is dominated by the plunge displacement which is evident from further analysis of time-domain plots that are not presented here [16]. The dominant scale associated with each response is initially low and corresponds to the high-frequency dynamics of the plunge mode. The presence of this dynamic is a result of the pitch-plunge coupling through the mass matrix in the equations of motion.

The transition at the end of Region I is caused by the decay of the plunge-mode response and an emerging dominance of the pitch-mode response. This early decay is a result of the larger damping in the plunge mode as compared to the pitch mode. The wavelet map demonstrates an increase in dominant scale to correspond with the decrease in frequency between between dominant modes.

The response in Region II is dominated by the dynamics of the pitch motion with only a small contribution from the coupled plunge motion so this data is useful for analyzing the dynamics of a single degree of freedom pitch system. The dominant scale, $\overline{a_i}$, demonstrates significantly different behavior for the wavelet analysis of the three systems as evident from Figure 5.

The constant scale $\overline{a_i}$ for the linear system response in Region II is directly indicative of linear system dynamics. The response in this Region results from a linear and time-invariant system with a single mode so the dominant frequency in the response should be constant and thus the dominant wavelet scale should be constant. The dominant scale has a value of $\overline{a_i} = 625$ and a corresponding frequency is computed as the sampling rate of 1000 *Hz* divided by this scale. The true frequency is then computed by normalizing the ratio by 1.2 which is the dominant wavelength of the Morlet wavelet. Thus the linearized responses shows a dominant frequency of 1.333 *Hz* which is similar to the predicted natural frequency of the pitch mode for the linear system.

The time-varying values of $\overline{a_i}$ associated with the responses in Region II from the system with a nonlinear hardening spring are considerably different than the scale for the linear system. Consider that the response from the system with a hardening spring initially shows a small dominant scale and increases with time. The effect of a hardening spring is to incur a larger restoring force at large amplitudes as compared to a linear spring. This force returns the system to the origin faster and consequently the response has a higher frequency for the nonlinear system. The difference between nonlinear and linear decreases as the response decays to a smaller amplitude and so the frequency in the responses becomes nearly identical. Thus, the wavelet maps reveal this behavior because an increasing scale is indicative of a decrease in frequency.

A similar analysis on the dominant scales associated with the response of the nonlinear system with the softening spring demonstrates the wavelet maps can detect and characterize this nonlinearity also. In this case, the softening spring results in a lower frequency in the response as compared to the linear system but the difference is small when the response amplitude is small. The dominant scale is initially larger for the response of the nonlinear system as compared to the linear system and decreases as time increases. Thus, the wavelet map reveals the initial frequency is lower in the response of the nonlinear system but it increases as the response decays to small amplitude.

The Region III analysis from Figure 5 notes the dominant scales, and consequently the frequency components, are similar for the responses from each system. This result is expected because the response magnitude has decayed as a result of damping and so each system can be approximated by the same linearized dynamics. The period of the dominant wavelet is $\overline{a_i} = 625$ which corresponds to a frequency of $\omega = 1.33\ Hz$ and matches the natural frequency of the linearized system.

The wavelet maps of the time responses are clearly indicative of nonlinearities under the assumptions of free-decay responses from single-mode, time-invariant systems. In particular, the responses in Region II reveal distinct differences between the responses of linear and nonlinear systems. Furthermore, these differences can be used to characterize the nature of the nonlinearities in the system dynamics.

4. Model Updating

This section presents the tool for parametric estimation of modal dynamics. A theoretical overview of the wavelet-based estimation is derived in terms of magnitude and phase characteristics. The μ method for flutter analysis is then discussed with respect to extending the baseline method to include the estimation tool. Robust flutter margins are generated for an F/A-18 using a nominal model and a model updated by the wavelet tool.

4.1. Parametric Modal Estimation

Consider $f(t) = k(t)\cos(\phi(t)t)$ as a general harmonic signal that may represent a typical sensor measurement. The corresponding wavelet transform, $F(a,\tau)$, can be analytically derived for a set of Morlet wavelets.

$$F(a,\tau) = \sqrt{a}k(t)e^{-(a\phi(t)-\omega_o)^2}e^{i\phi(t)\tau}$$

The modulus and phase of this wavelet transform are of interest because they indicate modal properties of the system. In particular, these quantities can be evaluated for a given scale, a_i, that corresponds to a natural frequency of the system.

$$\begin{aligned} |F(a_i,\tau)| &= \sqrt{a_i}k(t)e^{-(a_i\phi(t)-\omega_o)^2} \\ \angle[F(a_i,\tau)] &= \phi(t)\tau \end{aligned}$$

A concept of instantaneous frequency can be easily derived using the expression of phase of the wavelet transform [22]. This concept shows that a general time-varying envelope, $k(t)$, or time-varying phase, $\phi(t)$, of the signal can be determined from the modulus and phase of the wavelet transform for specific frequencies.

Flight data measured during flutter testing will often display features associated with viscously-damped, single degree of freedom systems. The corresponding envelope and phase functions can be explicitly written by noting that $f(t) = Ae^{-\zeta\omega_n t}\cos(\omega_d t + \phi_o)$ describes the measured signal. The corresponding wavelet expression for the envelope and instantaneous frequency for these systems can be formulated based on the general expression.

$$\begin{aligned} k(t) &= \frac{|F(a_i,\tau)|}{\sqrt{a_i}e^{-(a_i\phi(t)-\omega_o)^2}} &&= Ae^{-\zeta\omega_n t} \\ \phi(t)\tau &= \angle[F(a_i,\tau)] &&= \omega_d t + \phi_o \end{aligned}$$

The expression using phase of the wavelet transform indicates that the relationship between instantaneous frequency and damped natural frequency can be expressed as $\phi \approx \omega_d$. Similarly, the envelope decay rate can expressed as $\zeta\omega_n$. Thus, modal parameters of the system can be estimated by analyzing modulus and phase of the wavelet transform.

4.2. μ Method with Wavelet Processing

A method to compute stability margins of aeroservoelastic systems has been formulated based on robust stability theory[12]. This method uses a set of structured operators Δ, referred to as uncertainty, to describe errors and unmodeled dynamics in an analytical model. The structured singular value, μ, is used to compute a stability margin for this model that is robust, or worst-case, to the uncertainty operators[20].

The μ framework represents systems as operators with interconnections known as linear fractional transformations. This paper will use the notation $F(P,\Delta)$ to represent a feedback interconnection of the plant, P, and an associated uncertainty, Δ.

Flight data is incorporated into the μ method by formulating an uncertainty description that accounts for observed variations and errors[13]. A model validation analysis is performed on the plant model to ensure the range of dynamics admitted by the uncertainty is sufficient to cover the range observed with the flight data.

An ASE stability margin, Γ, is determined by computing μ with respect to an uncertainty description, $\delta_{\bar{q}}$, that admits variations in dynamic pressure and an uncertainty description, Δ, that describes modeling errors[14]. This margin relates the largest change in dynamic pressure that may be considered while guaranteeing the plant model is robustly stable to all errors described by Δ.

An implementation of the μ method with modal parameter estimation has been formulated that analyzes the wavelet maps of flight data to extract frequencies and dampings. A plant model, P_1, is computed by updating elements of the nominal plant model, P_0, with the modal parameter estimates. Only a limited subset of dynamics will be observed in the data so only a correspondingly limited subset of the plant modes will be updated. The parameters describing dynamics that are not observed by the data can not be estimated so the updated plant will directly use the nominal plant elements to describe these dynamics.

An uncertainty description, Δ_1, is generated for the plant with updated modal parameters, P_1, using a model validation procedure. This description will generally be smaller than the description associated with the nominal plant because the updated model should be more representative of the flight data. Essentially, the updated model is centered within the range of dynamics observed by the flight data.

The conservatism in robust margins computed by the μ method arises from excessive uncertainty descriptions needed to account for errors in a model. The decrease in uncertainty resulting from updating the model by the parameter estimation process may correspondingly decrease the conservatism in the robust stability margin.

4.3. F/A-18 HARV

Robust stability margins for the aeroservoelastic dynamics of the F/A-18 HARV are computed using the μ method with wavelet filtering. This aircraft, shown in Figure 6, is a twin-seat fighter that was modified to include thrust vectoring paddles on the engines and a research flight control system [21]. The flight system also included a method to generate excitation signals for measuring aeroservoelastic responses by summing programmed digital signals to the controller commands to the actuators [2]. Inputs from 5 to 25 *Hz* were added to the control surface commands at angles of attack from 5 to 70 deg of α at 1g.

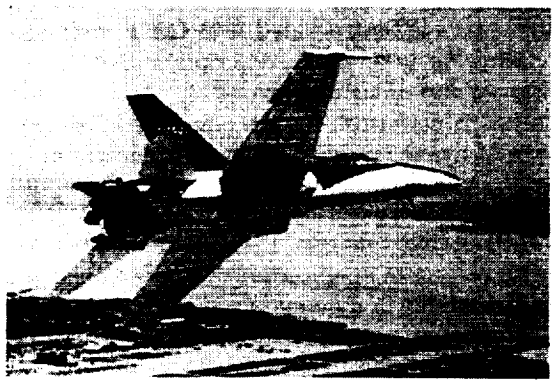

Figure 6: F/A-18 HARV

The μ method was used to analyze the stability margins at several points in the envelope; however, this paper will only consider the worst-case condition [18]. This worst-case margin is associated with the antisymmetric modes of the lateral-directional dynamics for the aircraft at Mach 0.3 and an altitude of 30000 *ft* with the dynamic pressure at $\bar{q} = 41$ lb/ft^2. The baseline μ method indicates an instability may lie close to the flight envelope so any reduction in conservatism could be significant.

A set of operators are used to indicate uncertainties in an analytical model. A complex operator, Δ_{in}, is a multiplicative uncertainty in the control inputs to the plant and accounts for actuator errors and unmodeled dynamics. Another complex operator, Δ_{add}, relates the control inputs to the feedback measurements to account for uncertainty in the magnitude and phase of the computed plant responses. The remaining operator, Δ_A, is a real parametric uncertainty affecting the modal parameters of the open-loop state matrix to describe errors in natural frequency and damping parameters.

The block diagram for robust stability analysis of the F/A-18 HARV aeroservoelastic dynamics is shown in Figure 7. This figure includes an operator, $\delta_{\bar{q}}$, that affects the nominal dynamics to describe changes in flight condition and is used to interpret μ as a stability margin [14]. Additional operators, W_{add} and W_{in}, are shown as weightings to normalize the frequency-varying uncertainty operators, Δ_{add} and Δ_{in}.

4.4. Models and Uncertainty

An initial model of the aircraft, P_0, is computed using 6 rigid-body modes and 10 antisymmetric structural modes along with 20 states associated with the unsteady aerodynamics. The control system adds 90 states to account for actuator dynamics and 29 states for the feedback controller.

An updated model, P_1, is computed by using modal parameter estimates to replace elements of the structural modes of P_0. These parameters are generated by analyzing the modulus and phase of the wavelet transform of accelerations measured in response to sine sweeps through the control surfaces. An uncertainty description, Δ_1, is derived to account for features in the data that can not be exactly reproduced by the updated model.

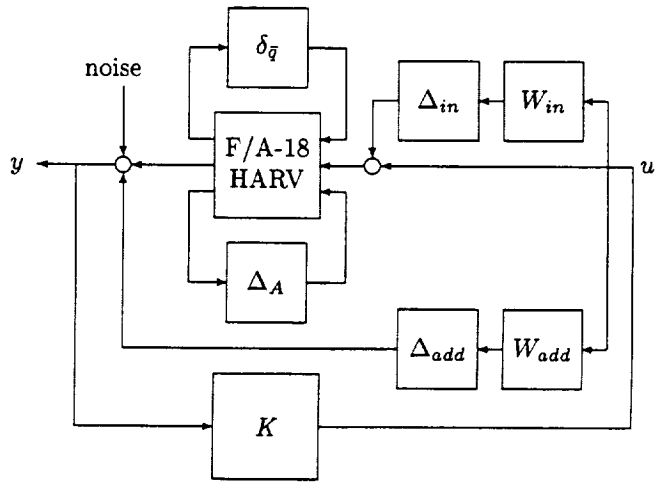

Figure 7: F/A-18 HARV Uncertainty Block Diagram for Robust Stability Margin Analysis

Table 2 presents an example of the modal properties for the original and updated models. The parameters are larger for the updated model than for the original model because the flight data indicates the theoretical values are too low. Consequently, the amount of variation in the parameters that results from uncertainty is considerably less for the updated model than for the original model. Note the absolute amount of variation in damping is actually greater for the updated model; however, the percentage of variation is less and this is the important consideration for this analysis.

model	ω (Hz)	ζ
$F(P_0, \Delta_0)$	$15.69 \pm .63$	$.010 \pm .007$
$F(P_1, \Delta_1)$	$16.51 \pm .35$	$.045 \pm .023$

Table 2: Modal Parameters and Uncertainty Variations for the Wing Fore-Aft Mode for Each Model

4.5. ASE Stability Margins

Nominal stability margins are computed for the plant model using the original theoretical modal parameters and the updated models using parameters estimated from wavelet filtering. These margins are computed from a μ analysis with respect to the variation in flight condition, $\bar{q}$, but ignoring the modal and complex uncertainty operators. The nominal stability margins, Γ, are given in Table 3 and demonstrate the largest decrease from the nominal dynamic pressure of $\bar{q} = 41$ lb/ft^2 that may be considered before the models incur an ASE instability.

model	Γ	ω
$F(P_0, 0)$	-268 lb/ft^2	14.8 Hz
$F(P_1, 0)$	-368 lb/ft^2	14.8 Hz

Table 3: Nominal Stability Margins for Each Model

The original theoretical model has a nominal stability margin of $\Gamma = -268\ lb/ft^2$ resulting from a critical instability of the wing fore-aft mode at 14.8 Hz. The margin is increased by updating the model with modal parameter estimates; however, the wing fore-aft mode remains the critical mode. This increase in stability margin associated with wavelet filtering is not guaranteed to occur for all applications; rather, the filtering is designed to make the nominal model more accurate. The nominal model for the F/A-18 HARV had low dampings so the wavelet filtering increased the modal damping levels and, in a sense, made the plant effectively more stable and increased the stability margins.

These nominal margins are all greater than the dynamic pressure at this flight condition so they demonstrate the nearest instability to the flight envelope occurs at a negative dynamic pressure, which is physically unrealizable. Thus, the nominal dynamics are free of ASE instabilities within the research flight envelope.

Robust stability margins are computed with respect to the uncertainty description of Figure 7 and given in Table 4. The original model and uncertainty description is represented by $F(P_0, \Delta_0)$ while the updated model with reduced uncertainty description is given by $F(P_1, \Delta_1)$.

model	Γ	ω
$F(P_0, \Delta_0)$	-4 lb/ft^2	15.4 Hz
$F(P_1, \Delta_1)$	-222 lb/ft^2	7.0 Hz

Table 4: Robust Stability Margins for Each Model

The stability margin of the original model is strongly affected by considering uncertainty. This margin is reduced from $\Gamma = -268\ lb/ft^2$ for the nominal dynamics to $\Gamma = -4\ lb/ft^2$ for the dynamics with respect to uncertainty. The critical mode remains the wing fore-aft mode despite the uncertainty; however, the dynamic pressure at which this mode becomes unstable is quite different. This robust stability margin demonstrates the nominal model may be misleading and the nearest unstable flight condition may actually lie close to the flight envelope.

The robust stability margin for the model $F(P_1, \Delta_1)$, which uses modal parameter estimates, is significantly larger than the margin of the original system. The wavelet processing is able to identify a more accurate model with less associated uncertainty so the conservatism in the margin is reduced. The robust stability margin for this model is $\Gamma = -222\ lb/ft^2$ and indicates the nearest instability for the updated model, despite the range of dynamics incurred by uncertainty, is at a negative dynamic pressure and so the flight envelope is robustly free of ASE instabilities.

The critical mode associated with the robust stability margin for the updated model is the first fuselage bending mode, which is different than the critical mode associated with the nominal margin. This shift in critical modes results from the inclusion of uncertainty that allows a variation to the fuselage dynamics that becomes unstable before the wing fore-aft mode. Similarly, the critical mode for the robust stability margin of the original model $F(P_0, \Delta_0)$ is the wing fore-aft mode, but the reduced uncertainty associated with $F(P_1, \Delta_1)$ shifts the critical mode so the variation in fuselage dynamics for the updated model encompasses the critical instability.

Comparison between the nominal results in Table 3 and the robust results of Table 4, both in Γ and modal frequency, clearly show the change in stability characteristics resulting from model updating and the corresponding uncertainty updating. The original model showed a substantial decrease in margin for the instability associated with the wing-fore aft mode when uncertainty was included. The updated model showed a much smaller decrease in margin despite the shift in modal instability. For this model, wing fore-aft modal frequency increased about 1 Hz from its theoretical value to the updated value and thereby became a less significant factor in the stability margin calculation compared with the fuselage mode. This result confirms that the effect of parameter estimation in model validation can be a critical factor for predicting robust stability margins.

5. Concluding Remarks

Wavelet analysis produces a time-frequency representation of data from which informative features may be extracted. This paper has shown several applications of wavelets that are valuable for flight flutter testing. A correlation filter is developed that can identify modal properties and indicate coupling and perhaps the onset of flutter during envelope expansion. Another application can be used to characterize nonlinearities in the system that may indicate behaviors such as limit cycle oscillations. Also, a method of modal parameter estimation is developed that can be used to update models and reduce conservatism in robust stability margins and allow envelope expansion to proceed to points that may be initially considered as dangerous because of excessive conservatism in original models.

References

[1] R. Bennett and I. Abel, "Application of a Flight Test and Data Analysis Technique to Flutter of a Drone Aircraft," *AIAA Structures, Structural Dynamics and Materials Conference*, Atlanta GA, AIAA-81-0652, April 1981.

[2] M.J. Brenner, *Aeroservoelastic Modeling and Validation of a Thrust-Vectoring F/A-18 Aircraft*, NASA TP-3647, September 1996.

[3] M.J. Brenner and E. Feron, "Wavelet Analysis of F/A-18 Aeroelastic and Aeroservoelastic Flight Test Data,". *AIAA Structures, Structural Dynamics, and Materials Conference*, AIAA 97-1216 and NASA TM-4793, April 1997.

[4] M. Brenner and R. Lind, "Wavelet-Processed Flight Data for Robust Aeroservoelastic Stability Margins," *Journal of Guidance, Control, and Dynamics*, Vol. 21, No. 6, November-December 1998, pp. 823-829.

[5] M. Brenner and R. Lind, "On-Line Aeroelastic Robust Stability Prediction using Wavelet Filtering," 21^{st} *Congress of the International Council of Aeronautical Sciences*, Melbourne, Australia, ICAS-98-4.9.1, September 1998.

[6] E. Dowell, "Nonlinear Aeroelasticity," *AIAA Structures, Structural Dynamics, and Materials Conference*, Long Beach CA, April 1990, AIAA-90-1031, pp. 1497-1509.

[7] E. Feron, M. Brenner, J. Paduano and A. Turevskiy, "Time-Frequency Analysis for Transfer Function Estimation and Application to Flutter Clearance," *Journal of Guidance, Control, and Dynamics*, Vol. 21, No. 3, May-June 1998, pp. 375-382.

[8] L. Freudinger, R. Lind and M. Brenner, "Correlation Filtering of Modal Dynamics using the Laplace Wavelet," *International Modal Analysis Conference*, Santa Barbara, CA, February 1998, pp. 868-877.

[9] G. Gilyard and J. Edwards, *Real-time Flutter Analysis of an Active Flutter Suppression System on a Remotely Piloted Research Aircraft*, NASA-TM-84901, January 1983.

[10] T. Kailath, *Linear Systems*, Prentice-Hall, Englewood Cliffs, NJ, 1980.

[11] M.W. Kehoe, "A Historical Overview of Flight Flutter Testing," *Proceedings of the* 80^{th} *AGARD Structures and Materials Panel*, AGARD-CP-566, Rotterdam, The Netherlands, May 8-10 1995, pp. 1-15.

[12] R. Lind and M. Brenner, *Robust Aeroservoelastic Stability Analysis*, Springer-Verlag, London, March 1999.

[13] R. Lind and M. Brenner, "Incorporating Flight Data into a Robust Aeroelastic Model," *Journal of Aircraft*, Vol. 35, No. 3, May-June 1998, pp. 470-477.

[14] R. Lind and M. Brenner, "Robust Flutter Margins of an F/A-18 Aircraft from Aeroelastic Flight Data," *Journal of Guidance, Control, and Dynamics*, Vol. 20, No. 3, May-June 1997, pp. 597-604.

[15] R. Lind, M. Brenner and L. Freudinger, "Improved Flight Test Procedures for Flutter Clearance," *International Forum on Aeroelasticity and Structural Dynamics*, Rome, Italy, June 1997, Volume 3, pp. 291-298.

[16] R. Lind, K. Snyder and M. Brenner, "Investigating Transient and Limit Cycle Behaviors of a Nonlinear Structure by Wavelet Transforms," *AIAA Structures, Structural Dynamics, and Materials Conference* Long Beach, CA, AIAA-98-1808, April 1998.

[17] R. Lind, K. Snyder and M. Brenner, "Wavelet Analysis to Characterize Nonlinearities and Predict Limit Cycles of an Aeroelastic System," *Mechanical Systems and Signal Processing*, accepted for publication.

[18] R. Lind and M. Brenner, "Analyzing Aeroservoelastic Stability Margins Using the μ Method," *AIAA Structures, Structural Dynamics, and Materials Conference*, Long Beach, CA, AIAA-98-1895, April 1998.

[19] T. O'Neil and T. Strganac, "Investigations of Aeroelastic Response for a System with Continuous Structural Nonlinearities," *AIAA Structures, Structural Dynamics, and Materials Conference*, Salt Lake City UH, April 1996, AIAA-96-1390.

[20] A.K. Packard and J.C. Doyle, "The Complex Structured Singular Value," *Automatica*, Vol. 29, No. 1, 1993, pp. 71-109.

[21] J.W. Pahle, B. Powers, V. Regenie, V. Chacon, S. Degroote and S. Murnyack, *Research Flight Control Development for the F-18 High-Alpha Research Vehicle*, NASA TM-104232, 1991.

[22] M. Ruzzene, A. Fasana, L. Garibaldi, and B. Piombo, "Natural Frequencies and Dampings Identification using Wavelet Transform: Application to Real Data," *Mechanical Systems and Signal Processing*, Vol. 11, No. 2, 1997, pp. 207-218.

[23] W.J. Staszewski, "Identification of Nonlinear Systems using Multi-Scale Ridges and Skeletons of the Wavelet Transform," *Journal of Sound and Vibration*, Vol. 214, No. 4, 1998, pp. 639-658.

[24] G. Strang and T. Nguyen, *Wavelets and Filter Banks*, Wellesley-Cambridge Press, 1996.

[25] J. Thompson and H. Stewart, *Nonlinear Dynamics and Chaos*, John Wiley and Sons, Chichester England, 1986.

[26] S. Wiggins, *Introduction to Applied Nonlinear Dynamical Systems and Chaos*, Springer-Verlag, New York NY, 1990.